Title
New insight into the interaction of TRAF2 C-terminal domain with lipid raft microdomains

Journal
Biochimica et Biophysica Acta (BBA) - Molecular and Cell Biology of Lipids, 1862(9)

ISSN
1388-1981

Authors
Ceccarelli, Arianna
Di Venere, Almerinda
Nicolai, Eleonora
et al.

Publication Date
2017-09-01

DOI
10.1016/j.bbalip.2017.05.003

BBA - Molecular and Cell Biology of Lipids 1862 (2017) 813–822

Contents lists available at ScienceDirect

BBA - Molecular and Cell Biology of Lipids

journal homepage: www.elsevier.com/locate/bbalip

New insight into the interaction of TRAF2 C-terminal domain with lipid raft microdomains

Arianna Ceccarelli[a,1], Almerinda Di Venere[a,c,1], Eleonora Nicolai[a], Anastasia De Luca[a], Nicola Rosato[a,c], Enrico Gratton[b], Giampiero Mei[a,c,*], Anna Maria Caccuri[a,c,*]

[a] Department of Experimental Medicine and Surgery, University of Rome Tor Vergata, Via Montpellier 1, 00133 Rome, Italy
[b] Laboratory for Fluorescence Dynamics, Biomedical Engineering Department, University of California at Irvine, Irvine, CA, USA.
[c] Center NAST, Nanoscience, Nanotechnology, Innovative Instrumentation, University of Rome Tor Vergata, 00133 Rome, Italy

ARTICLE INFO

Keywords:
Fluorescence microscopy
General Polarization
Lipid rafts
Protein–lipid interaction

ABSTRACT

In this study we provide the first evidence of the interaction of a truncated-TRAF2 with lipid raft microdomains. We have analyzed this interaction by measuring the diffusion coefficient of the protein in large and giant unilamellar vesicles (LUVs and GUVs, respectively) obtained both from synthetic lipid mixtures and from natural extracts. Steady-state fluorescence measurements performed with synthetic vesicles indicate that this truncated form of TRAF2 displays a tighter binding to raft-like LUVs with respect to the control (POPC-containing LUVs), and that this process depends on the protein oligomeric state. Generalized Polarization measurements and spectral phasor analysis revealed that truncated-TRAF2 affects the membrane fluidity, especially when vesicles are heated up at physiological temperature. The addition of nanomolar concentration of TRAF2 in GUVs also seems to exert a mechanical action, as demonstrated by the formation of intraluminal vesicles, a process in which ganglioside GM1 plays a crucial role.

1. Introduction

The TNF receptor-associated factor (TRAF) proteins interact with and transduce signals for members of the TNF receptor superfamily. TRAFs are characterized by an oligomeric structure that plays a fundamental role in the binding process with membrane receptors. To date, six members of the TRAF family have been found and among them TRAF2 is the most ubiquitously expressed and widely studied member. Human TRAF2 is characterized by a highly conserved carboxy-terminal TRAF domain, which can be further subdivided into a TRAF-C domain and a coiled coil region named TRAF-N domain. The carboxy-terminal TRAF domain mediates homo- or hetero-oligomerization among the TRAF family and the interactions with upstream receptors (including TNFR1, TNFR2, CD40 and CD30) and a number of adapters and signaling molecules. The TRAF2 amino-terminal region contains a RING finger and several zinc-finger motifs that appear critical for downstream signaling. In particular, it has been demonstrated that clustering of the amino-terminal effector domains is sufficient for activating MEKK1 and the downstream protein kinases that transduce TNF-α and IL-1 signals [1].

We have recently demonstrated that a truncated-TRAF2 may also exist as a stable monomer and this population is the predominant species when TRAF2 is in the nanomolar concentration range. Therefore, the monomer–trimer equilibrium can be crucial for regulating the activities of TRAF2 in vivo [2].

The subcellular localization of TRAF2 in intact cells is another crucial point and, in fact, it has been investigated in detail by several authors. Hostager and colleagues [3] reported that TRAF2 is distributed throughout the cytoplasm of unstimulated mouse B cells (lymphocytes), while CD40 engagement causes a very rapid recruitment of both TRAF2 and CD40 to detergent-insoluble microdomains named membrane rafts [4–6]. Of note, in addition to the interaction of the carboxy-terminal TRAF domain of TRAF2 to the cytoplasmic domain of CD40 [7] it has been also reported that the zinc-binding regions of TRAF2 may contribute to its recruitment to raft microdomains likely interacting with membrane raft-associated molecules.

Abbreviations: TRAF, TNF receptor-associated factor; JNK, c-Jun N-terminal kinase; LUV, large unilamellar vesicles; GUVs, giant unilamellar vesicles; BBMs, brush border membranes; DOPC, 1,2-dioleoyl-*sn*-glycero-3-phosphocholine; POPC, 1-palmitoyl-2-oleoyl-*sn*-glycero-3-phosphocholine; GM1, monosialotetrahexosylganglioside; Laurdan, 6-lauroyl,1-2-dimethylamino naphthalene; FCS, fluorescence correlation spectroscopy; sFCS, scanning FCS measurements; GP, General Polarization; ID, intestinal duodenum; IJ, intestinal jejunum; SC, kidney superficial cortex; JMC, kidney juxtamedullary cortex; SPA, spectral phasor analysis; UPR, unfolded protein response

* Corresponding authors at: Department of Experimental Medicine and Surgery, University of Rome Tor Vergata, Via Montpellier 1, 00133 Rome, Italy.
E-mail addresses: mei@med.uniroma2.it (G. Mei), caccuri@uniroma2.it (A.M. Caccuri).
[1] These authors equally contributed to this research.

http://dx.doi.org/10.1016/j.bbalip.2017.05.003
Received 20 September 2016; Received in revised form 2 May 2017; Accepted 6 May 2017
Available online 09 May 2017

The TRAF2 translocation is crucial for its activation and for downstream signaling events and is heavily regulated by ubiquitin signals [8–9]. Habelhah and coworkers [10] demonstrated that TNFα-induced ubiquitination of TRAF2, by the ubiquitin-conjugating enzyme Ubc13, resulted in its translocation to the insoluble membrane/cytoskeletal fraction [10] and this also coincided with the TRAF2 ability to induce activation of c-Jun N-terminal kinase (JNK), but neither p38 nor NF-kB were affected by the extent of TRAF2 ubiquitination.

Moreover, several evidences prove a relation between TRAF2 signaling and the ER compartment: TRAF2 is not only an indispensable mediator in the activation of JNK by TNF-α [11] but is also a key player of ER stress-induced JNK activation [12].

Finally, TRAF2 may reside in the nucleus and directly regulate transcription, independently of its role in cytoplasmic signal transduction. TRAF2 has been recently reported to be localized in the nuclear compartment of hESC cells, and its interaction with nuclear CD30v, a variant of CD30 receptor, has been suggested to drive NF-κB activation [13]. There is indeed further evidence that TRAF2 can enter the nucleus and interact with specific gene promoters [14].

Therefore, several lines of evidence suggest that targeting TRAF2 to specific compartments may be the major determinant in the TRAF2 ability to activate distinct downstream signaling cascades. Lipid raft microdomains are known to play a major role in various aspects of intracellular trafficking and signal transduction and play also a crucial role in the TRAF2 compartmentalization. However, little is known about the molecular details of TRAF2 interaction with these regions; in particular it is not completely clear whether TRAF2 binding requires its trimerization and interaction with the activated receptor or if TRAF2 may directly bind to lipid rafts in the oligomeric or monomeric form.

In the present study we analyzed in detail the interaction of the C-terminal domain (residues 310–501) of TRAF2 with lipid raft microdomains by using fluorescence spectroscopy and two-photon fluorescence microscopy. For this purpose, large and giant unilamellar vesicles (LUVs and GUVs, respectively) generated from different lipid mixtures have been used as a model system mimicking lipid raft rich membranes. In particular we employed three kinds of synthetic vesicles of increasing complexity and POPC-liposomes for control experiments. POPC, being particularly abundant in animal cell membranes, has been previously used as a major component to study the L_d phase in model membranes. Indeed, an exam of the T-P phase diagram of different phospholipid bilayer systems [15] and the analysis of ternary mixtures phase diagrams [16] revealed that POPC vesicles at $P = 1$ atm and $T = 25$ °C are in a single fluid phase, thus representing the simplest model of liquid-disordered bilayers. A more complex model membrane used in this study is based on the ternary mixture DOPC/sphingomyelin/cholesterol (1/1/1), which provides vesicles in which liquid-ordered and liquid-disordered phases coexist [17]. Such a system mimics raft-containing membranes and therefore has been extensively studied and characterized in the past with several techniques, ranging from fluorescence spectroscopy [18], to atomic force microscopy [19]. Finally, we have also used ex-vivo reconstituted GUVs, namely model bilayers, obtained from the natural lipids present in brush border membranes (BBMs) that are considered a rich source of putative rafts [20]. Our experiments prove that TRAF2, mainly in the monomeric form, is able to directly bind to raft-containing GUVs, affecting the fluidity of the bilayer. Moreover, our study reveals a peculiar property of TRAF2: the presence of this protein causes an increase in the number of intra-luminar vesicles, suggesting that it might exert a mechanical action on the membrane.

2. Materials and methods

2.1. Chemicals

1,2-Dioleoyl-*sn*-glycero-3-phosphocholine (DOPC), 1-palmitoyl-2-oleoyl-*sn*-glycero-3-phosphocholine (POPC), cholesterol, brain sphingomyelin, and ovine ganglioside GM1 (GM1) were purchased from Avanti Polar Lipids (Birmingham, AL). Alexa Fluor 488 labeling kit, 6-lauroyl,1-2-dimethylamino naphthalene (Laurdan) and CellMask Orange were purchased from Invitrogen (Carlsbad, CA).

2.2. Expression and purification of TRAF2

E. coli BL21 (DE3) cells were transformed with the His-tagged human TRAF2 C-terminal domain (residues 310–501) construct and grown in Luria broth medium containing 30 μg/ml kanamicin sulfate. Expression of TRAF2 was induced by the addition of 1 mM isopropyl-1-thio-β galactopyranoside. After 18 h at 25 °C, cells were harvested, re-suspended in lysis buffer (20 mM Tris-HCl pH 8.0, 150 mM NaCl, 20 mM imidazole, 10% glycerol, 1 mM DTT and EDTA-free inhibitor of protease) and sonicated. The cellular extract was loaded on a 10 ml Ni-NTA column pre-equilibrated with lysis buffer and the protein was eluted using a linear gradient consisting of 50 ml of lysis buffer and 50 ml of the same buffer containing 500 mM imidazole. Imidazole was then removed from the TRAF2 sample by filtration through a Sephadex G25 column (GE Healthcare Life Science, Chalfont St. Giles, UK) pre-equilibrated with the Kinase Buffer (KB, 20 mM Tris-HCl pH 7.6 containing 150 mM NaCl and 10% glycerol). The TRAF2 content and its purity were analyzed in the eluted fractions by SDS-PAGE. Protein concentration was determined by measuring the absorbance at 280 nm and using an extinction coefficient of 17,780 $M^{-1}\,cm^{-1}$ for TRAF2 monomers. Proteins were stored at −80 °C. The final protein concentration for LUV and GUV experiments was in the range 0.5–10 μM and 15–30 nM, respectively.

2.3. Lipid extraction from brush border membranes

Brush border membranes (BBMs) were provided by Prof. Moshe Levi, University of Colorado, Denver. Briefly BBMs from kidney superficial cortex (SC), kidney juxtamedullary cortex (JMC), intestinal duodenum (ID), and intestinal jejunum (IJ) of adult rats were isolated and purified by the differential centrifugation and magnesium precipitation gradient method [21–22]. Total lipids were extracted from BBMs by the method of Bligh and Dyer [21,23].

2.4. Preparation of LUVs and GUVs

LUVs were prepared as previously described [24] and laurdan incorporated before vesicle formation (final lipid concentration 1 mM; final laurdan concentration 50 μM). GUVs were prepared by the electroformation method developed by Angelova and Dimitrov [25–26] in a special Teflon temperature-controlled chamber, designed by Bagatolli and Gratton [27].

Five microliters of lipid stock solution (0.3 mg/ml in chloroform for synthetic mixtures) were spread on each of the two platinum wires. After waiting for 15 min (30 min for BBMs), to let the solvent's residues evaporate, 800 μl of 200 mM sucrose solution were added. Both the chamber and the solution were pre-warmed up to 10° above the highest phase transition temperature for the given lipid mixture. Therefore, different temperatures were utilized: room temperature for POPC, 60 °C for lipid raft mixture, while for all the BBMs, temperature was set at 42 °C. Platinum wires were then connected to a wave generator and a sinusoidal wave was applied. Briefly we used two different steps in the electroformation procedure. The first step, which lasts 30 min, corresponds to an increase of the field amplitude E, at fixed frequency f, up to its maximum value E_{max}; during the second step (30 min) electric field parameters ($E = E_{max}$ and f) were kept constant [28].

For scanning fluorescence correlation spectroscopy (sFCS) and imaging, GUVs were stained using CellMask Orange: stock solution of probe was diluted 100 fold and 2 μl of the working solution was added to the sucrose solution. Measurements were performed after 15 min to let the probe insert into the membrane.

Table 1
Binding parameters of TRAF2 to different synthetic membranes at 25 °C and Generalized Polarization values (cf. Materials and methods).

	[TRAF2] ≈ 0.7 μM		[TRAF2] ≈ 8.5 μM		GP [TRAF2] = 0	GP [TRAF2] ≈ 0.7 μM
	[a]$[L_{1/2}]$ (μM)	[b]$\Delta F_{max}/F_0$	$[L_{1/2}]$ (μM)	$\Delta F_{max}/F_0$		
POPC	28 ± 2	0.86 ± 0.06	61 ± 4	0.52 ± 0.04	− 0.120 ± 0.005	− 0.094 ± 0.006
POPC + GM1	23 ± 1	0.83 ± 0.05	60 ± 4	0.51 ± 0.04	− 0.130 ± 0.006	− 0.153 ± 0.007
DOPC/SM/CHOL	20 ± 1	0.65 ± 0.03	34 ± 3	0.54 ± 0.04	0.320 ± 0.007	0.385 ± 0.007
					[c]0.266 ± 0.008	[c]0.192 ± 0.006

[a] $[L_{1/2}]$ = Lipid concentration at which 50% of saturation is achieved.
[b] F_0 = protein fluorescence intensity in the absence of liposomes; ΔF_{max} = maximum fluorescence change.
[c] Values obtained at 37 °C.

For Generalized Polarization (GP) measurements the Laurdan labeling procedure was done adding 10 μl of a 1 mM Laurdan solution in dimethylsulfoxide before the vesicle formation.

2.5. Linear scanning FCS measurement and imaging

Confocal images and linear sFCS were performed on an Olympus Fluoview 1000 microscope (Olympus, Tokyo, Japan) equipped with an Olympus UplanSApo 60 × (1.20 NA) water objective. Excitation was from the 488 nm laser line of a 40 mW Arion laser (Melles-Griot, Carlsbad, CA). Fluorescence emission was split by a dichroic mirror at 560 nm and detected in the 505–525 nm (AlexaFluor 488) and 575–675 nm (CellMask Orange) spectral ranges. Correlation curves have been fitted using a 3D-Gaussian intensity profile distribution.

Images of 256 × 256 pixels were collected and 100 frames were recorded. For sFCS the excitation laser beam was rapidly directed in a uniform linear scan across GUV membranes [29]. The line was 128 pixels long and the zoom was 24 ×. A pixel dwell time of 8 μs/pixel was set for both imaging and sFCS. Data were collected through the Olympus Fluoview 1000 software and analyzed with SimFCS (a routine developed at the LFD) [19].

2.6. Steady-state fluorescence measurements

The decrease in the steady-state TRAF2 intrinsic fluorescence, due to the energy transfer effect upon TRAF2 binding to laurdan-containing LUVs, was measured on a K2-ISS spectrofluorometer (ISS, Champaign, IL, USA). Measurements were carried on at two fixed TRAF2 concentrations, upon excitation at 275 nm, increasing the amount of vesicles in the solution. Each spectrum was corrected by the dilution factor and by inner filter effects and the total intrinsic fluorescence intensity, F_L, obtained evaluating the spectral area in the range 295–400 nm. Then, the change of the emission intensity, $\Delta F = F_L - F_0$ (being F_0 the initial fluorescene in the absence of liposomes) was plotted as a function of lipid concentration $[L]$, and fitted according to: $\Delta F = \Delta F_{max} \frac{[L]}{[L]_{1/2} + [L]}$ where ΔF_{max} and $[L]_{1/2}$ are the asymptotic change in fluorescence (at infinite lipid concentration) and the lipid concentration at which $\Delta F = 1/2\ \Delta F_{max}$, respectively [30].

2.7. Generalized Polarization measurements

The acquisition of fluorescence spectra images of GUVs was performed on a Zeiss LSM 710 microscope (Carl Zeiss, Jena, Germany) using a 40 × water immersion objective, 1.2 N.A. (Carl Zeiss, Oberkochen, Germany). For the 2-photon excitation laser source, a titanium:sapphire MaiTai laser (Spectra-Physics, Mountain View, CA) was used with excitation at 780 nm. Image scan speed was 177.32 μs/pixel and image size is 256 × 256 pixels. 32 spectra were collected in the 416–727 nm range (each spectrum had a width of 9.7 nm). To evaluate the Generalized Polarization of the images acquired, we considered spectra from 1 to 6 for the blue region and from 7 to 15 for the green region. GP function is a ratiometric approach, which takes into account the difference between the fluorescence intensity at two different wavelengths, divided by their sum:

$$GP = \frac{I_{Blue} - I_{Green}}{I_{Blue} + I_{Green}}$$

However, since GP values obtained from the GP images strongly depend on instrumental parameters, such as filter settings and gain used in the microscope, the system was calibrated with a correcting factor G [31]. The measurement of the factor G was performed by acquiring images of a Laurdan reference solution (100 μM in dimethylsulfoxide), with a known GP, using the same instrumental conditions as in the membrane experiments. Therefore, the GP equation used to calculate the GP images becomes:

$$GP = \frac{I_{Blue} - (G^* I_{Green})}{I_{Blue} + (G^* I_{Green})}$$

2.8. Statistical analysis

Statistical analysis was performed by the nonparametric Mann–Whitney U test, analyzing experimental data by means of the Prism 5 program (GraphPAD Software for Science, San Diego, CA, USA). Unless otherwise specified, the data reported in Table 1 and in the figures are the mean (± S.D.) of at least three independent determinations.

The results were considered to be statistically significant at $P < 0.05$.

3. Results

3.1. Diffusion coefficient measurements using linear sFCS

In order to investigate whether TRAF2 interacts directly with membranes, the Alexa-labeled protein was monitored by fluorescence microscopy, in the presence of POPC-GUVs (Fig. 1). Then, sFCS across the GUV lipid bilayer was performed. This approach allows for a straightforward detection of spatial-temporal interactions between the protein and the membrane, based on the diffusion rate of the protein [29]. In the sFCS the laser beam is repetitively and rapidly directed in a uniform linear scan across the GUV's membrane. Thus, an output “carpet” of timed fluorescence intensity fluctuations, at specific points along the scan, is recorded and a typical result is reported in Fig. 2. Briefly, on the left side (Fig. 2a, channel-1) the carpet obtained in the “spectral window” of the Alexa Fluor 488 is shown, while in a parallel acquisition (Fig. 2b, channel-2) the signal of the CellMask Orange (a membrane marker) was recorded as a control. In these plots each vertical column of the carpet represents the fluctuation in time of the fluorescence signal observed in a specific position in space [29]. Thus, a set of autocorrelation curves can be extracted, the typical trend being reported in Fig. 2c. A fit of each autocorrelation curve under different experimental conditions yields the average diffusion coefficient of the labeled particle traveling through the lipid bilayer. This approach has

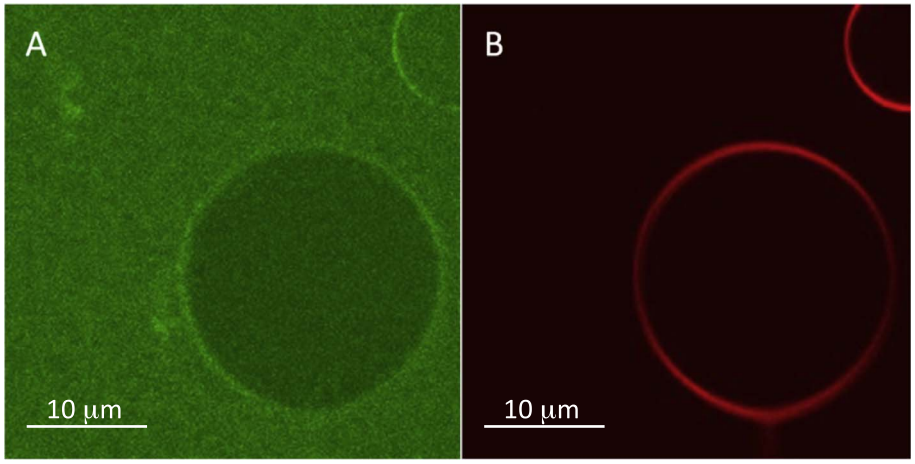

Fig. 1. Panel a: binding of Alexa-labeled TRAF2 to a POPC-GUV (diameter 20 μm); panel b: visualization of the GUV through the membrane marker CellMask Orange. Measurements were performed using a confocal microscope (see Materials and methods section).

been repeated using different model vesicles and the diffusion coefficient of TRAF2 obtained in each case (averaging a minimum of 4–5 trials) is shown in Fig. 3. As a control, experiments were performed using POPC vesicles to test the binding of TRAF2 to fluid membranes [32]. The diffusion coefficient obtained in this case was D_{POPC} = (0.8 ± 0.2) μm^2/s, compatible with the diffusion values of proteins in membranes reported in literature [33]. When raft-containing GUVs were taken into account, the average diffusion coefficient of ALEXA-labeled TRAF2 decreased to D_{RAFT} = (0.3 ± 0.1) μm^2/s, showing a slower dynamics.

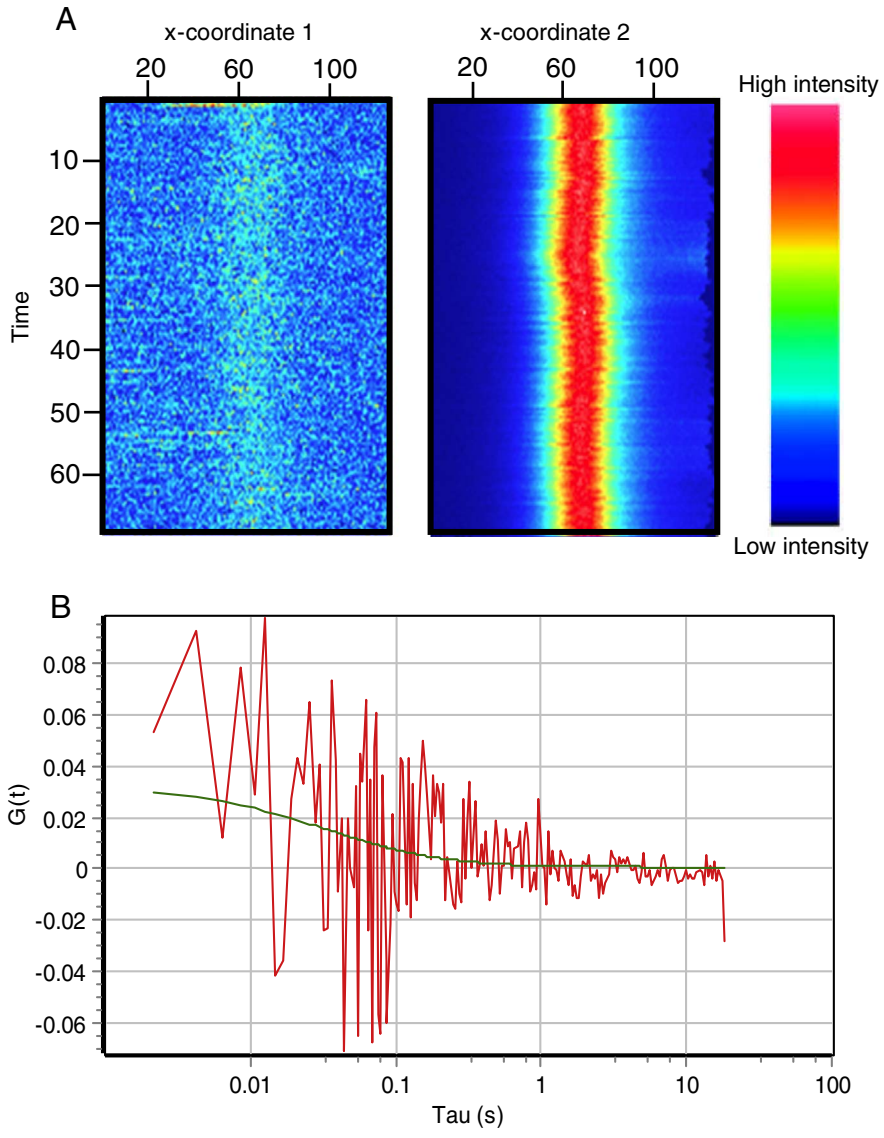

Fig. 2. Scanning FCS intensity carpet of Alexa 488-TRAF2 (Panel a, left) and CellMask Orange (Panel a, right) along the scanning line of a POPC GUV. Panel b: fitted autocorrelation curves of Alexa 488-TRAF2.

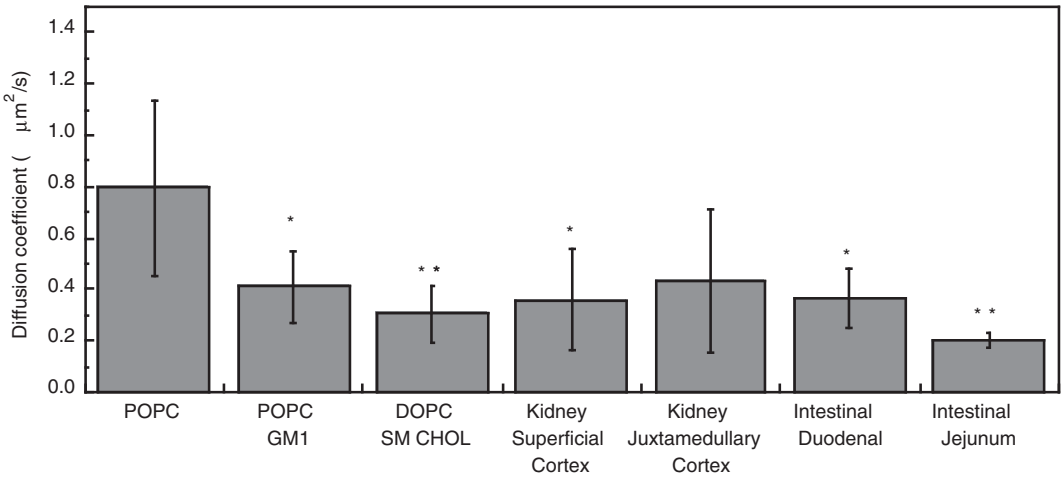

Fig. 3. Diffusion coefficients of labeled TRAF2 bound to GUVs. Vesicles were obtained from 1-palmitoyl-2-oleoyl-*sn*-glycero-3-phosphocholine (POPC), raft-like mixture (i.e. 1,2-dioleoyl-*sn*-glycero-3-phosphocholine/sphingomyelin/cholesterol (DOPC/SM/cholesterol), BBM samples (kidney juxtamedullary cortex (JMC), kidney superficial cortex (SC), intestinal duodenum (ID), and intestinal jejunum (IJ)) and POPC + 1% GM1. Data are expressed as mean ± SD values of three independent experiments; * and ** denote $p < 0.05$ and $p < 0.01$, respectively, versus TRAF2 bound to POPC-GUVs.

Recently, it has been demonstrated that gangliosides such as GM1 can modulate the order/disorder phase in synthetic membranes [34]. Since this glycosphingolipid is known to co-localize indirectly with TRAF2 in natural membranes, via the TNF-receptor [35], we also characterized the diffusion of TRAF2 in POPC-GUVs containing 1% of GM1. The result obtained demonstrates that the diffusion coefficient ($0.4 \pm 0.1\ \mu m^2/s$) is indeed of the same order as that found in the raft-containing GUVs, suggesting that a direct interaction with the ganglioside might take place. Very low diffusion rates (in the range $0.2–0.43\ \mu m^2/s$) were also obtained in the presence of GUVs reconstituted from brush border membrane (BBM) vesicles (Fig. 3). This finding is in line with the high content of lipid rafts expected in these model membranes [36].

3.2. TRAF2 binding to synthetic vesicles

The binding of TRAF2 to lipid bilayers has been characterized measuring the fluorescence energy transfer effect from the protein tryptophans to laurdan-containing LUVs of different compositions. The main parameters obtained fitting the data ($[L]_{1/2}$ and ΔF_{max}, see Materials and methods) are reported in Table 1. The results indicate that the protein preferentially binds to complex vesicles rather than simple POPC liposomes, the lowest $[L]_{1/2}$ value being obtained in the case of LUVs made composed of a ternary lipid mixture. A second important finding concerns the dependence on the TRAF2 concentration: both $[L]_{1/2}$ and $\Delta F_{max}/F_0$ values suggest that a more efficient binding process takes place when the protein is more diluted. According to the TRAF2 dissociation constant [2], the decrease of protein concentration from 8.5 to 0.7 μM, leads to an increase in the fraction of monomers (from 5% to 20% respectively) with respect to the trimers, thus suggesting that the dissociated subunits display an enhanced propensity to bind membranes.

Another important feature of the interaction between TRAF2 and lipid bilayers has been observed performing measurements on laurdan-containing vesicles. Laurdan is a fluorescent probe [7] sensitive to the polarity of the surrounding environment, being therefore particularly suitable to study membrane packing and lipid order [37]. Laurdan spectral shifts are essentially due to the re-orientation of water molecules along the probe excited state dipole [37], a process that depends only on the phase state of the lipid bilayer. In particular, in the liquid–crystalline phase the readjustment of water molecules determines the red shift of the emission spectrum, while gel phase phospholipid bilayers do not exhibit any changes in the emission. Such changes can be quantified using the GP function (see Materials and methods) that can discriminate the gel and the liquid-crystalline phases of the membrane [38], the highest GP values corresponding to the most ordered lipid bilayer states.

In this study we performed measurements of Laurdan-containing LUVs and GUVs both at room temperature (25 °C) and at physiological temperature (37 °C), before and after the addition of non-labeled TRAF2. The results, reported in Table 1 and Fig. 4, demonstrate that in some cases (ID and IJ derived GUVs) the GP value was higher at room temperature than at physiological temperature. This finding was expected, since there is a direct relationship between temperature and membrane fluidity.

Interestingly, in the case of brush border membranes derived from JMC and in synthetic vesicles simulating raft-containing lipid bilayers, an opposite trend was observed (Fig. 4). This behavior is characteristic of high cholesterol content, whose peculiar properties might in principle explain such “anomalous” dependence on temperature. In fact the cholesterol steroid ring is closely attracted to part of the fatty acid chain of the nearest-neighbor phospholipid, probably hindering the solidification at low (room) temperature [39]. In contrast, at physiological temperature, cholesterol promotes the immobilization of the outer surface of the membrane, which becomes less permeable to small solutes that generally diffuse through the lipid bilayer [39].

When unlabeled TRAF2 was added to fluid synthetic membranes (POPC-GUVs), the GP value increased at both temperatures, providing evidence of a direct action of TRAF2 in affecting the fluidity of the bilayer (Fig. 4). The GP value was also higher in the presence of the protein in the case of SC-BBM, ID-BBM and IJ-BBM. In contrast, a much larger and opposite effect was observed at 37 °C, both in the case of raft- and GM1-containing GUVs and in JMC-BBM. Further studies are needed to explain these results.

3.3. Spectral phasor analysis

The GP characterization of membrane fluidity is based on the sample fluorescence intensity at two different wavelengths. However, each pixel of an image intrinsically contains much more spectral information that can be used to separate ordered from disordered lipid phases. This task can be easily achieved performing a spectral phasor analysis (SPA), in which the main features of the spectrum collected at each point of the image (center of mass and width) are summarized in a “phasor plot” [40]. It has been found that synthetic lipids containing two phases display almost linear phasor plots, each pixel being the

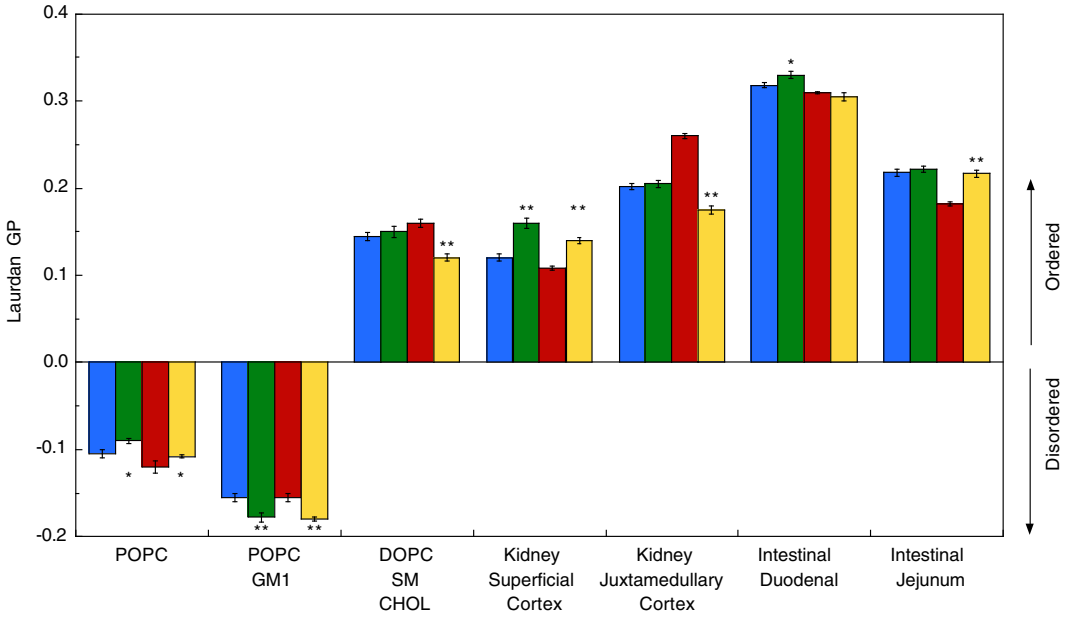

Fig. 4. Laurdan GP values calculated at room temperature (blue and green) and body temperature (red and yellow) for all samples, before (blue and red) and after the addition of non-labeled TRAF2 (green and yellow). Data are expressed as mean ± SD values calculated from at least 15–20 GUVs of two different preparations. * and ** denote $p < 0.05$ and $p < 0.01$, of green and yellow samples versus the blue and red ones, respectively.

result of a linear combination of the two spectral components. In the case of natural membranes the complexity of the system increases, due to the presence of multiple kinds of interactions within the lipid bilayer, and the pattern of the phasor diagram might assume a non-linear shape [41]. The effects of TRAF2 on membrane fluidity have been therefore characterized using this approach. In particular, images of different Laurdan-containing model membranes are reported in a false color representation, at 25 °C, in Fig. 5. The color code has been obtained as follows. In the right side (panels B, E, H, M), the corresponding polar phasor plot has been divided in seven areas represented by non-overlapped colored circles of equal size. Each point falling within a determined circle corresponds to a pixel of the image having those specific spectral features (center of mass and width) collected in the images on the left. Thus, pixels with the same color correspond to points falling in the same colored ring of the phasor plot.

According to this representation, red circles in the phasor plot (or red pixel in the images) correspond to Laurdan molecules emitting in the long wavelength range (diagnostic of a liquid-disordered phase), while purple rings (and pixels) represent bluer-emitting probes (indicating the presence of lateral ordered lipids). This feature is particularly evident in control measurements that parallel the results found in the GP analysis (Fig. 4). In fact, while simple, disordered GUVs (POPC) appears in orange, GM1-containing GUVs are red colored, indicating an increased disorder degree, in line with the results of GP analysis (Fig. 4). In contrast to simple GUVs, synthetic raft-like membranes are characterized by blue-colored pixels, suggesting the presence of more organized lipid bilayers. On the other hand, the colors of GUVs obtained from BBMs span from mostly green (SC) to purple (ID), such heterogeneity arising from the different kind of tissues of origin. Indeed, membranes with a high GP value such as ID-GUVs (Fig. 4) are also characterized by a small angular position in the phasor plot, falling therefore in the purple ring (Fig. 5A), indicating a particularly ordered lipid bilayer.

The addition of unlabeled TRAF2 (25 nM) produced different effects, depending on the type of membrane. For instance, in the case of ID and SC GUVs, the color code adopted suggests that protein binding induced a stiffening of the lipid bilayer, both at 25 °C and at 37 °C. This is particularly evident for the ID sample in which some of the pixels colored in purple turned to pink, populating a more “ordered” area of the phasor plot (Fig. 5A, B, right). Another striking feature of TRAF2 binding to BBMs extracted from intestinal duodenum is the conversion of a very fluid portion of the membrane (represented by a yellow spot) in a more rigid environment, as suggested by the blue-shift of the image pixels, at both temperatures.

As already observed in the GP analysis (Fig. 4), an opposite trend characterized the presence of TRAF2 in JMC and raft-like GUVs. In particular, in these cases the pixel density in the phasor plot decreased in the smaller wavelength range of Laurdan emission (blue ring area), shifting to larger ones (green and yellow ring areas).

Finally, the effects of TRAF2 binding to IJ GUVs displayed a more complex behavior, being temperature-dependent: a more fluid bilayer is induced at room temperature, while stiffening is achieved at 37 °C.

3.4. Vesiculation of GUVs after TRAF2 addition

A novel finding of the interaction between TRAF2 and lipid bilayers regards the protein capability of inducing vesiculation. This feature was qualitatively studied monitoring the time-dependent effect of TRAF2 on a model membrane containing artificial lipid rafts. After a few minutes of protein addition in solution, the GUVs exhibited an increase in the number of intra-luminar vesicles, suggesting that the protein might indeed exert a mechanical action on the membrane (Fig. 6). Measurements have then been repeated in the case of the other model membranes and the data quantitatively analyzed measuring the vesicle numbers and their average diameter before and after the addition of the protein. For each experiment performed, around sixty GUVs were measured and observed before and after the addition of TRAF2. Control experiments have also been carried on in the presence of KB (see Materials and methods), in order to exclude an osmotic contribution to vesicle formation due to the buffer content of NaCl. Moreover, measurements were repeated before and after the addition of BSA 25 nM, which does not affect the GUV structure in this condition, as previously demonstrated [42]. Indeed, the data reported in Fig. 7 demonstrate that vesiculation occurs in all samples after TRAF2 addition, while BSA does not induce significant modification of the model membranes studied. Interestingly, vesiculation in POPC GUVs dramatically depends on the presence of the glycosphingolipid GM1 (1 mol%), suggesting that in natural membranes it could play a crucial role in driving this

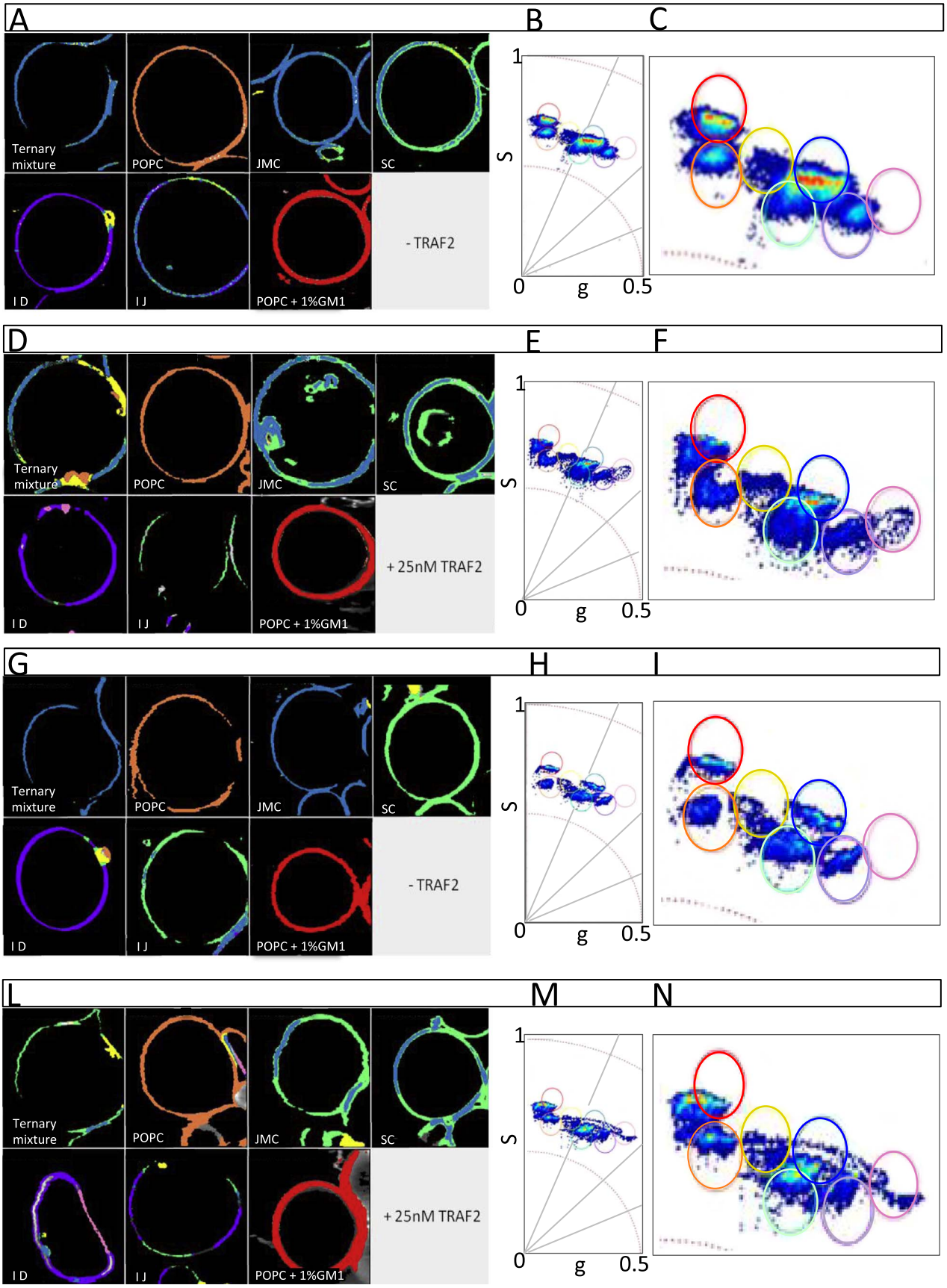

Fig. 5. GUV images acquired at room temperature (panels A, D) or at body temperature (lower panels G and L) before and after the addition of non-labeled TRAF2. The corresponding spectral phasor plots of the GUVs are reported in panels B, E, H, M and, with enlarged scale, in C, F, I, and N. The color of each pixel in the GUV image depends on the phasor position. The diameter of the GUVs varied from 20 to 50 μm. The membranes used in each experiment (panels A, D, G, L), starting from the upper left corner proceeding clockwise, are the ternary mixture DOPC/SM/cholesterol, POPC, JMC, SC, POPC + 1% GM1, IJ, and ID.

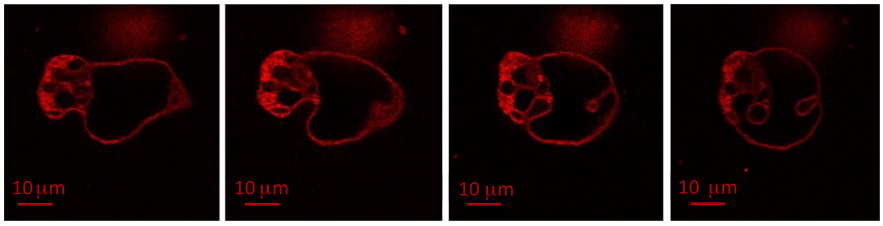

Fig. 6. Vesicle formation on a raft-like GUV followed in time. The estimated diameter of the GUV is ≈ 30 μm. After the addition of TRAF2, the GUV showed an increase in the number of intraluminar vesicles. Images have been obtained from a movie, at intervals of about 10 s.

phenomenon.

3.5. Incorporation in the vesicles of free dye after addition of TRAF2

A further confirmation of TRAF2-induced vesiculation has been obtained adding the fluorescent dye Alexa-488 (86 μM) to the solution of preformed GUVs, before the injection of TRAF2. In this way, thanks to the dye fluorescence emission, it was possible to monitor the formation of new vesicles within the GUV lumen. Indeed, in Fig. 8B (left panel) the appearance of Alexa-filled small vesicles after TRAF2 addition validates the protein-induced mechanical effects.

4. Discussion

Lipid rafts are liquid-ordered phase microdomains in membranes. They represent glycosphingolipid- and cholesterol-rich lipid regions, in which lipid acyl chains are tightly packed and highly extended. Such packed arrangement of lipids and the consequent neat phase separation within the bilayer is probably responsible for their insolubility in non-ionic detergents. They have been proven to play an important role in many signaling pathways [6], through different mechanisms. For example they may contain incomplete signaling pathways that are activated after recruiting the requisite components of signaling into the raft itself. In other cases they may limit signaling, either by physical segregation of signaling components to avoid nonspecific interactions, or by modulating the intrinsic activities of proteins located within them. In particular, they are involved in TRAF2 recruiting, which then causes JNK activation and subsequently cell death [43].

Lipid rafts have been implicated in transport routes of endoplasmic reticulum [44] and several evidences prove a relation between TRAF2 signaling and the ER compartment. In particular, TRAF2 has been reported to mediate in the ER a pathway similar to that initiated by cell surface receptors in response to extracellular signals like TNFα [12,45]. In the ER lumen, transmembrane and secreted proteins are folded and post-translationally modified, the ER being a major site of passage for proteins directed to other organelles, to the cell surface, and to the extracellular space. Misfolded proteins in the ER activate the unfolded protein response (UPR), a protective cellular response. Moreover,

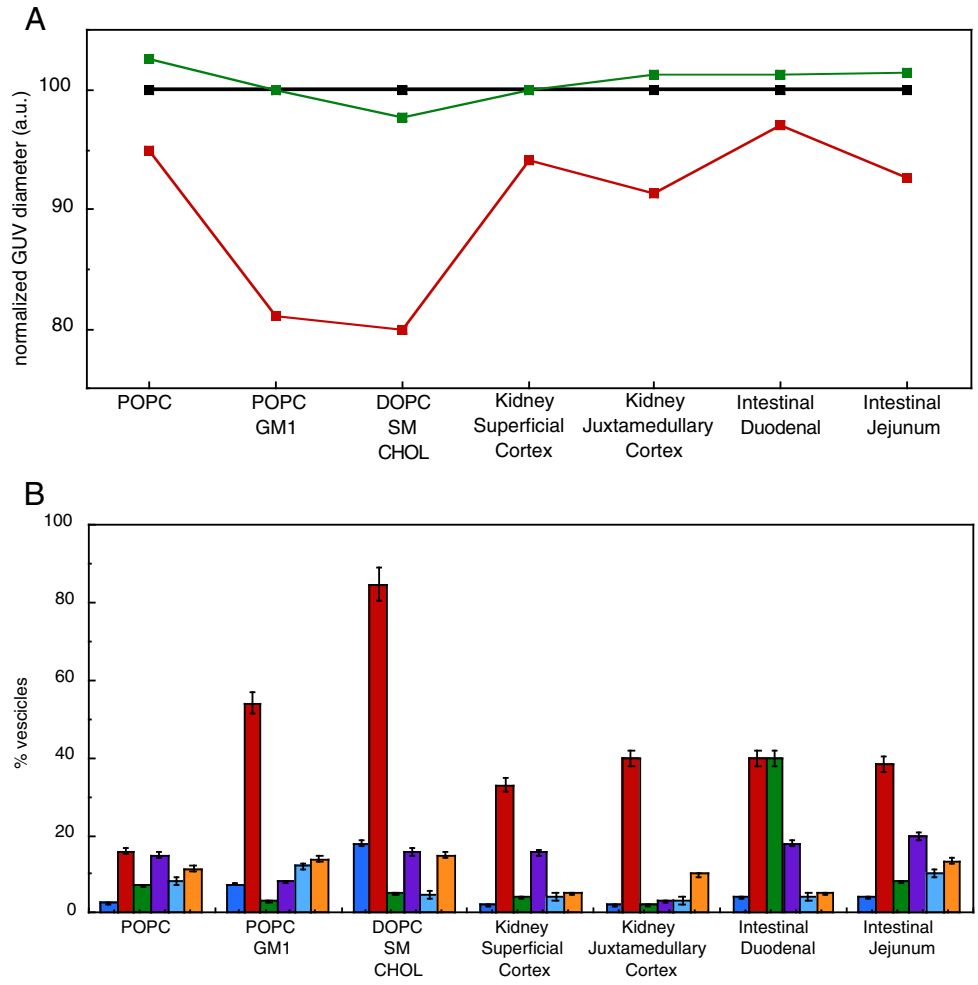

Fig. 7. Panel A: GUV diameter changes observed after TRAF2 addition (red). Control experiments have been conducted adding KB (black horizontal line) and BSA (green). Points have been connected only to guide the eye. Panel B: percentage of intraluminal vesicles occurring in GUVs in the absence of TRAF2 (blue, green, cyan), after TRAF2 addition (red) and in control experiments in which KB (purple) or BSA (orange) have been added.

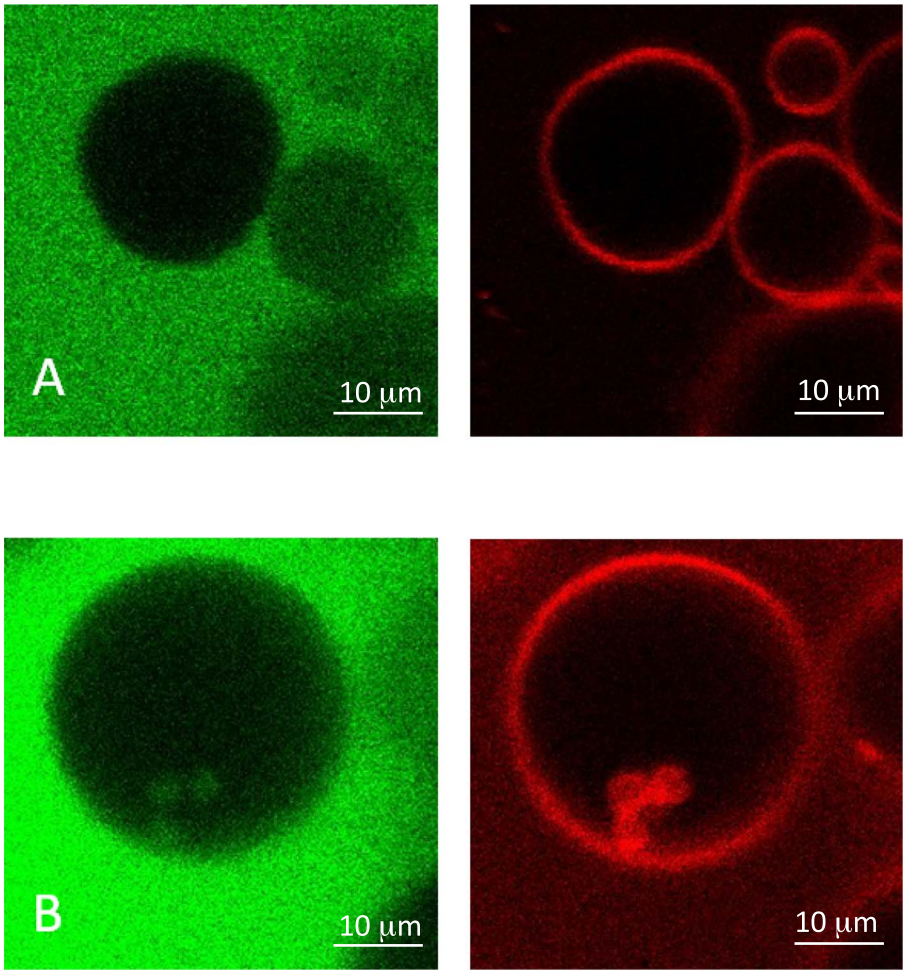

Fig. 8. Panel A: JMC GUVs surrounded by free dye, before adding 25 nM of TRAF2. Panel B: Alexa 488-filled vesicles formed upon the addition of 25 nM non-labeled TRAF2. The diameters of the GUVs are 20–30 μm.

several viruses bud into the ER-Golgi compartment where mutated viral envelope proteins are retained provoking ER stress and UPR, which are the major determinants of neurovirulence [46]. Stress signals from the ER are transduced by inositol requiring kinase 1 (IRE1). This protein recruits TRAF2 to the ER membrane, leading to the initiation of multiple signaling pathways, such as JNK activation, required for the activation of apoptosis under irreversible ER stress [12].

In this paper we have provided evidence of the interaction between the C-terminal domain of TRAF2 and unilamellar vesicles (LUVs and GUVs) containing artificial lipid rafts. We have shown that the protein, especially in the monomeric form, displays a higher propensity in binding liposomes that resemble the lipid raft composition. This finding supports the hypothesis that the monomer–trimer equilibrium could play a crucial role in regulating the binding of TRAF2 to biological membranes [2]. The time course analysis of the truncated-TRAF2 interaction with these membranes also reveals that the protein exerts a mechanical action on the lipid bilayer, as shown by the rapid increase in the number of intra-luminar vesicles entrapped. In addition, our results show that the ganglioside GM1 strongly favors this process and therefore it might be directly involved in the binding of truncated-TRAF2 to GUVs. In this case, we can speculate that the most flexible region in truncated TRAF2 monomers (i.e. the N-terminal α-domain) [47] might be responsible for the interaction with the ganglioside.

GM1 plays a crucial role in the endocytic uptake into cells of polyoma viruses and some bacterial toxins [48]. Moreover, excessive accumulation of GM1 in lysosomes of mouse neurons has been reported to cause GM1 increase at the ER membrane, which in turn activates the apoptotic pathway [49]. Overall, our data, showing that GM1 synergizes with truncated-TRAF2 to induce vesiculation, may bridge the gap between GM1 accumulation at the ER membrane and activation of the ER stress response.

Indeed, the possibility that a truncated C-terminal form of TRAF2 may exist inside the cells as a result of a partial degradation of TRAF2 cannot be ruled out. In support to this hypothesis is the evidence that recruitment of TRAF2 to the insoluble fraction is often linked to its rapid degradation. Confocal microscopy experiments showed that after TNF-R2 activation, TRAF2 and the E3 ligase c-IAP1 translocate to a Triton X-100 (TX)-insoluble region that is localized in the ER. This compartmentalization plays a key role for TRAF2 ubiquitination and subsequent degradation in a proteasome-dependent manner [50].

The ubiquitin-proteasome pathway functions not only in the complete degradation of polypeptides, but also in the regulated processing of precursors into active proteins [51–53]. Therefore, we can hypothesize that a partial degradation TRAF2 may occur in response to ER stress and may play an important role in this process. These unexpected findings may extend our current understanding of the roles and mechanisms of action of TRAF2. In particular, our data might allow hypothesizing a role for a truncated form of TRAF2 in the multivesicular body (MVB) pathway [54] that favors the transport of misfolded and damaged proteins from ER to the sites of their breakdown [55].

Transparency document

The http://dx.doi.org/10.1016/j.bbalip.2017.05.003 associated with this article can be found, in the online version.

Acknowledgements

EG was supported by grants from the National Institute of Health NIH P41-GM103540 and NIH P50-GM076516. AMC was supported by a grant from Consolidate the Foundations 2015.

We would like to dedicate this study to the memory of Carmine Di Rienzo, a brilliant scientist who tragically passed away a few months ago and who has been of invaluable help for A. Ceccarelli during her stage at the LFD.

References

[1] V. Baud, Z.G. Liu, B. Bennett, N. Suzuki, Y. Xia, M. Karin, Signaling by proinflammatory cytokines: oligomerization of TRAF2 and TRAF6 is sufficient for JNK and IKK activation and target gene induction via an amino-terminal effector domain, Genes Dev. 13 (10) (1999) 1297–1308.
[2] A. Ceccarelli, A. Di Venere, E. Nicolai, A. De Luca, V. Minicozzi, N. Rosato, A.M. Caccuri, G. Mei, TNFR-Associated Factor-2 (TRAF2): not only a trimer, Biochemistry 54 (40) (2015) 6153–6161.
[3] B.S. Hostager, I.M. Catlett, G.A. Bishop, Recruitment of CD40 and tumor necrosis factor receptor-associated factors 2 and 3 to membrane microdomains during CD40 signaling, J. Biol. Chem. 275 (20) (2000) 15392–15398.
[4] D.A. Brown, E. London, Structure and function of sphingolipid- and cholesterol-rich membrane rafts, J. Biol. Chem. 275 (23) (2000) 17221–17224.
[5] B.A. Tsui-Pierchala, M. Encinas, J. Milbrandt, E.M. Johnson Jr., Lipid rafts in neuronal signaling and function, Trends Neurosci. 25 (8) (2002) 412–417.
[6] K. Simons, D. Toomre, Lipid rafts and signal transduction, Nat. Rev. Mol. Cell Biol. 1 (1) (2000) 31–39.
[7] G. Weber, F.J. Farris, Synthesis and spectral properties of a hydrophobic fluorescent probe: 2-dimethylamino-6-propionylnaphthalene, Biochemistry 18 (1979) 3075–3078.
[8] S.Y. Lee, A. Reichlin, A. Santana, K.A. Sokol, M.C. Nussenzweig, Y. Choi, TRAF2 is essential for JNK but not NF-kappaB activation and regulates lymphocyte proliferation and survival, Immunity 7 (5) (1997) 703–713.
[9] M. Takeuchi, M. Rothe, D.V. Goeddel, Anatomy of TRAF2. Distinct domains for nuclear factor-kappaB activation and association with tumor necrosis factor signaling proteins, J. Biol. Chem. 271 (33) (1996) 19935–19942.
[10] H. Habelhah, S. Takahashi, S.G. Cho, T. Kadoya, T. Watanabe, Z. Ronai, Ubiquitination and translocation of TRAF2 is required for activation of JNK but not of p38 or NF-kappaB, EMBO J. 23 (2) (2004) 322–332.
[11] W.C. Yeh, A. Shahinian, D. Speiser, J. Kraunus, F. Billia, A. Wakeham, J.L. de la Pompa, D. Ferrick, B. Hum, N. Iscove, P. Ohashi, M. Rothe, D.V. Goeddel, T.W. Mak, Early lethality, functional NF-kappaB activation, and increased sensitivity to TNF-induced cell death in TRAF2-deficient mice, Immunity 7 (5) (1997) 715–725.
[12] F. Urano, X. Wang, A. Bertolotti, Y. Zhang, P. Chung, H.P. Harding, D. Ron, Coupling of stress in the ER to activation of JNK protein kinases by transmembrane protein kinase IRE1, Science 287 (5453) (2000) 664–666.
[13] N.Y. Thakar, D.A. Ovchinnikov, M.L. Hastie, B. Kobe, J.J. Gorman, E.J. Wolvetang, TRAF2 recruitment via T61 in CD30 drives NFκB activation and enhances hESC survival and proliferation, Mol. Biol. Cell 26 (5) (2015) 993–1006.
[14] W. Min, J.R. Bradley, J.J. Galbraith, S.J. Jones, E.C. Ledgerwood, J.S. Pober, The N-terminal domains target TNF receptor-associated factor-2 to the nucleus and display transcriptional regulatory activity, J. Immunol. 161 (1) (1998) 319–324.
[15] R. Winter1, W. Dzwolak2, Exploring the temperature–pressure configurational landscape of biomolecules: from lipid membranes to proteins, Phil. Trans. R. Soc. A 363 (2005) 537–563, http://dx.doi.org/10.1098/rsta.2004.1507.
[16] D. Marsh, Cholesterol-induced fluid membrane domains: a compendium of lipid-raft ternary phase diagrams, Biochim. Biophys. Acta 1788 (2009) 2114–2123.
[17] N. Kahya, Targeting membrane proteins to liquid-ordered phases: molecular self-organization explored by fluorescence correlation spectroscopy, Chem. Phys. Lipids 141 (1–2) (2006) 158–168.
[18] C. Nicolini, A. Celli, E. Gratton, R. Winter, Pressure tuning of the morphology of heterogeneous lipid vesicles: a two-photon-excitation fluorescence microscopy study, Biophys. J. 91 (2006) 2936–2942.
[19] C. Yuan, J. Furlong, P. Burgos, P.J. Johnston, The size of lipid rafts: an atomic force microscopy study of ganglioside GM1 domains in sphingomyelin/DOPC/cholesterol membranes, Biophys. J. 82 (May 2002) 2526–2535.
[20] G.H. Hansen, L. Immerdal, E. Thorsen, L.L. Niels-Christiansen, B.T. Nystrøm, E.J. Demant, E.M. Danielsen, Lipid rafts exist as stable cholesterol-independent microdomains in the brush border membrane of enterocytes, J. Biol. Chem. 276 (34) (2001) 32338–32344.
[21] M. Levi, B.A. Molitoris, T.J. Burke, R.W. Schrier, F.R. Simon, Effects of vitamin D-induced chronic hypercalcemia on rat renal cortical plasma membranes and mitochondria, Am. J. Phys. 252 (2 Pt 2) (1987) F267–F275.
[22] B.A. Molitoris, F.R. Simon, Renal cortical brush-border and basolateral membranes: cholesterol and phospholipid composition and relative turnover, J. Membr. Biol. 83 (3) (1985) 207–215.
[23] E.G. Bligh, W.J. Dyer, A rapid method of total lipid extraction and purification, Can. J. Biochem. Physiol. 37 (8) (1959) 911–917.
[24] F. Sinibaldi, L. Milazzo, B.D. Howes, M.C. Piro, L. Fiorucci, F. Polticelli, P. Ascenzi, M. Coletta, G. Smulevich, R. Santucci, The key role played by charge in the interaction of cytochrome *c* with cardiolipin, J. Biol. Inorg. Chem. 22 (1) (2017) 19–29.
[25] M.I. Angelova, S. Soléau, P. Méléard, F. Faucon, P. Bothorel, Preparation of giant vesicles by external AC electric fields. Kinetics and applications, Progr. Colloid Polym. Sci. 89 (1992) 127–131.
[26] M.I. Angelova, D.S. Dimitrov, Liposome electroformation, Faraday Discuss. Chem. Soc. 81 (1986) 303–311.
[27] L.A. Bagatolli, E. Gratton, Two-photon fluorescence microscopy observation of shape changes at the phase transition in phospholipid giant unilamellar vesicles, Biophys. J. 77 (4) (1999) 2090–2101.
[28] P. Méléard, L.A. Bagatolli, T. Pott, Giant unilamellar vesicle electroformation from lipid mixtures to native membranes under physiological conditions, Methods Enzymol. 465 (2009) 161–176.
[29] Q. Ruan, M.A. Cheng, M. Levi, E. Gratton, W.W. Mantulin, Spatial-temporal studies of membrane dynamics: scanning fluorescence correlation spectroscopy (SFCS), Biophys. J. 87 (2) (2004) 1260–1267.
[30] G. Mei, A. Di Venere, E. Nicolai, C.B. Angelucci, I. Ivanov, A. Sabatucci, E. Dainese, H. Kuhn, M. Maccarrone, Structural properties of plant and mammalian lipoxygenases. Temperature-dependent conformational alterations and membrane binding ability, Biochemistry 47 (2008) 9234–9242.
[31] K. Gaus, E. Gratton, E.P. Kable, A.S. Jones, I. Gelissen, L. Kritharides, W. Jessup, Visualizing lipid structure and raft domains in living cells with two-photon microscopy, Proc. Natl. Acad. Sci. U. S. A. 100 (26) (2003) 15554–15559.
[32] N. Kučerka, M.P. Nieh, J. Katsaras, Fluid phase lipid areas and bilayer thicknesses of commonly used phosphatidylcholines as a function of temperature, Biochim. Biophys. Acta 1808 (11) (2011) 2761–2771.
[33] J.D. Knight, M.G. Lerner, J.G. Marcano-Velázquez, R.W. Pastor, J.J. Falke, Single molecule diffusion of membrane-bound proteins: window into lipid contacts and bilayer dynamics, Biophys. J. 99 (9) (2010) 2879–2887.
[34] N. Puff, C. Watanabe, M. Seigneuret, M.I. Angelova, G. Staneva, Lo/Ld phase coexistence modulation induced by GM1, Biochim. Biophys. Acta 1838 (8) (2014) 2105–2114.
[35] I. Hunter, G.F. Nixon, Spatial compartmentalization of tumor necrosis factor (TNF) receptor 1-dependent signaling pathways in human airway smooth muscle cells. Lipid rafts are essential for TNF-alpha-mediated activation of RhoA but dispensable for the activation of the NF-kappaB and MAPK pathways, J. Biol. Chem. 281 (45) (2006) 34705–34715.
[36] C. Dietrich, L.A. Bagatolli, Z.N. Volovyk, N.L. Thompson, M. Levi, K. Jacobson, E. Gratton, Lipid rafts reconstituted in model membranes, Biophys. J. 80 (3) (2001) 1417–1428.
[37] T. Parasassi, E.K. Krasnowska, L.A. Bagatolli, E. Gratton, Laurdan and Prodan as polarity-sensitive fluorescent membrane probes, J. Fluoresc. 8 (4) (1998) 365–373.
[38] W. Yu, P.T. So, T. French, E. Gratton, Fluorescence generalized polarization of cell membranes: a two-photon scanning microscopy approach, Biophys. J. 70 (2) (1996) 626–636.
[39] H. Lodish, A. Berk, S.L. Zipursky, P. Matsudaira, D. Baltimore, J. Darnell, Molecular Cell Biology, fourth ed., W.H.Freeman And Company, New York, NY, 2000, pp. 451–463.
[40] M.A. Digman, V.R. Caiolfa, M. Zamai, E. Gratton, The phasor approach to fluorescence lifetime imaging analysis, Biophys. J. 94 (2) (2008) L14–L16.
[41] O. Golfetto, E. Hinde, E. Gratton, The Laurdan spectral phasor method to explore membrane micro-heterogeneity and lipid domains in live cells, Methods Mol. Biol. 1232 (2015) 273–290.
[42] F. Ruggeri, A. Akesson, P.Y. Chapuis, C.A. Skrzynski Nielsen, M.P. Monopoli, K.A. Dawson, T.G. Pomorski, M. Cárdenas, The dendrimer impact on vesicles can be tuned based on the bilayer charge and the presence of albumin, Soft Matter 9 (37) (2013) 8862–8870.
[43] Y.-T. Wu, S. Zhang, Y.-S. Kim, H.-L. Tan, M. Whiteman, C.-N. Ong, Z.-G. Liu, H. Ichijo, H.-M. Shen, Signaling pathways from membrane lipid rafts to JNK1 activation in reactive nitrogen species-induced non-apoptotic cell death, Cell Death Differ. 15 (2008) 386-39.
[44] E. Ikonen, Roles of lipid rafts in membrane transport, Curr. Opin. Cell Biol. 13 (4) (2001) 470–477.
[45] H. Nishitoh, M. Saitoh, Y. Mochida, K. Takeda, H. Nakano, M. Rothe, K. Miyazono, H. Ichijo, ASK1 is essential for JNK/SAPK activation by TRAF2, Mol. Cell 2 (3) (1998) 389–395.
[46] S.W. Chan, The unfolded protein response in virus infections, Front. Microbiol. 5 (2014) 518.
[47] A. De Luca, G. Mei, N. Rosato, E. Nicolai, L. Federici, C. Palumbo, A. Pastore, M. Serra, A.M. Caccuri, The fine-tuning of TRAF2-GSTP1-1 interaction: effect of ligand binding and in situ detection of the complex, Cell Death Dis. 5 (2014) e1015.
[48] H. Ewers, A. Helenius, Lipid-mediated endocytosis, Cold Spring Harb. Perspect. Biol. 3 (8) (2011) a004721.
[49] A. Tessitore, P.M.M. del, R. Sano, Y. Ma, L. Mann, A. Ingrassia, E.D. Laywell, D.A. Steindler, L.M. Hendershot, A. d'Azzo, GM1-ganglioside-mediated activation of the unfolded protein response causes neuronal death in a neurodegenerative gangliosidosis, Mol. Cell 15 (2004) 753–766.
[50] C.J. Wu, D.B. Conze, X. Li, S.X. Ying, J.A. Hanover, J.D. Ashwell, TNF-alpha induced c-IAP1/TRAF2 complex translocation to a Ubc6-containing compartment and TRAF2 ubiquitination, EMBO J. 24 (10) (2005) 1886–1898.
[51] T. Hoppe, K. Matuschewski, M. Rape, S. Schlenker, H.D. Ulrich, S. Jentsch, Activation of a membrane-bound transcription factor by regulated ubiquitin/proteasome-dependent processing, Cell 102 (5) (2000) 577–586.
[52] E.K. Schrader, K.G. Harstad, R.A. Holmgren, A. Matouschek, A three-part signal governs differential processing of Gli1 and Gli3 proteins by the proteasome, J. Biol. Chem. 286 (45) (2011) 39051–39058.
[53] V.J. Palombella, O.J. Rando, A.L. Goldberg, T. Maniatis, The ubiquitin-proteasome pathway is required for processing the NF-kappa B1 precursor protein and the activation of NF-kappa B, Cell 78 (5) (1994) 773–785.
[54] R.C. Piper, D.J. Katzmann, Biogenesis and function of multivesicular bodies, Annu. Rev. Cell Dev. Biol. 23 (2007) 519–547.
[55] S. Wang, G. Thibault, D.T. Ng, Routing misfolded proteins through the multivesicular body (MVB) pathway protects against proteotoxicity, J. Biol. Chem. 286 (33) (2011) 29376–29387.